Fast Solving Method Based on Linearized Equations of Branch Power Flow for Coordinated Charging of EVs (EVCC)

Jian Zhang, Mingjian Cui, *Senior Member, IEEE*, Bing Li, Hualiang Fang, and Yigang He, *Member, IEEE*

***Abstract*—Reported researches on smart charging methods have the disadvantages of low calculation efficiency or have not simultaneously taken the three-phase imbalance, voltage and power flow constraints into account. It is an important topic to improve the computational speed to meet the online rolling optimization requirement for EVCC problems. In this paper, the branch power flow equations of balanced and unbalanced distribution system are derived. The linearization methods for the nonlinear terms of the branch power flow equations are proposed. Two stages linear programming (LP) is introduced for EVCC to minimize the total charging costs of the holders where three-phase imbalance, charging demand, voltage and power flow constraints have been taken into account. Via ignoring the nonlinear terms of the branch power flow equations, the first stage LP is formulated to calculate the estimated branch power and node voltages as the initial points for linearizing the nonlinear terms of branch power flow equations. The second stage LP is formulated to calculate the optimal charging power using the linearized branch power flow equations. Four case studies show that the proposed method without the compromise of precision is significantly faster than state-of-the-art works with respect to the computational speed.**

***Index Terms*—Branch flow, distribution system, coordinated charging, electric vehicles (EVs), linear programming.**

NOMENCLATURE

A. Sets:

$\mathbb{N}$	Buses of distribution system excluding the root node.
ε	Line segments of distribution system.
H_k	Child nodes of node k.

B. Constants:

r_{ik}	Resistance of line segment (i,k) for balanced distribution system.
x_{ik}	Reactance of line segment (i,k) for balanced distribution system.
z_{ik}	Impedance of line segment (i,k) for balanced distribution system.
$\boldsymbol{r}_{ik}$	Resistance matrix of line segment (i,k) for unbalanced distribution system, a 3×3 matrix.
$\boldsymbol{x}_{ik}$	Reactance matrix of line segment (i,k) for unbalanced distribution system, a 3×3 matrix.
$\boldsymbol{z}_{ik}$	Impedance matrix of line segment (i,k) for unbalanced distribution system, a 3×3 matrix.
p^{d}_{k0}	Active power of constant power load at node k for balanced distribution system.
q^{d}_{k0}	Reactive power of constant power load at node k for balanced distribution system.
p^{d}_{kz0}	Active power of constant impedance load at node k for balanced distribution system when voltage magnitude is 1.0 p.u.
q^{d}_{kz0}	Reactive power of constant impedance load at node k for balanced distribution system when voltage magnitude is 1.0 p.u.
$\boldsymbol{p}^{\mathrm{d}}_{k0}$	Active power of constant power load at node k for unbalanced distribution system, a 3×1 vector.
$\boldsymbol{q}^{\mathrm{d}}_{k0}$	Reactive power of constant power load at node k for unbalanced distribution system, a 3×1 vector.
$\boldsymbol{p}^{\mathrm{d}}_{kz0}$	Active power of constant impedance load at node k for unbalanced distribution system, a 3×1 vector.
$\boldsymbol{q}^{\mathrm{d}}_{kz0}$	Reactive power of constant impedance load at node k for unbalanced distribution system, a 3×1 vector.
K	Total number of EVs with three-phase charging mode.
M	Total number of EVs with single-phase charging mode.
t_1	Optimization start time.
$t_{\max}$	Optimization end time.
β	Connecting phase for EVs with single-phase charging mode.
$P_{\mathrm{EV}k,\max}$	Charging power for the k^{th} EV with three-phase charging mode.
$P_{\mathrm{EV}m,\max}$	Charging power for the m^{th} EV with single-phase charging mode.
Δt	Time interval of optimization.
η	Charging efficiency.
E^{ini}_k	Initial energy of the k^{th} EV with three-phase charging mode.
E^{ini}_m	Initial energy of the m^{th} EV with single-phase charging mode.
E^{cap}_k	Battery capacity of the k^{th} EV with three-phase charging mode.
E^{cap}_m	Battery capacity of the m^{th} EV with single-phase charging mode.
$t_{k\mathrm{s}}$	Charging start time for the k^{th} EV with three-phase charging mode.
$t_{k\mathrm{e}}$	Charging end time for the k^{th} EV with three-phase charging mode.

J. Zhang, B. Li, and Y. He are with the School of Electrical Engineering and Automation, Hefei University of Technology, Hefei, Anhui, 230009 China; Y. He is also with the School of Electrical Engineering, Wuhan University, Wuhan, Hubei, 430072 China (e-mail: 17775357967@163.com; libinghnu@163.com; 18655136887@163.com).

M. Cui is with the Department of Electrical and Computer Engineering, Southern Methodist University, Dallas, TX, 75275 USA (e-mail: mingjian.cui@ieee.org).

H. Fang is with the School of Electrical Engineering, Wuhan University, Wuhan, Hubei, 430072 China (e-mail: hlfang@whu.edu.cn).

Manuscript received, 2019.

t_{ms} Charging start time for the m^{th} EV with single-phase charging mode.
t_{me} Charging end time for the m^{th} EV with single-phase charging mode.
$U_{\min}$ Lower limit for voltage magnitude square.
$U_{\max}$ Upper limit for voltage magnitude square.
$P_{ik,\alpha,t}^{\max}$ Maximum active power of line segment (i,k) for phase α in time interval t.
$P_{\mathrm{T},\alpha,t}^{\max}$ Maximum active power of distribution transformer for phase α in time interval t.
P_{ik0} Initial active power of line segment (i,k) for linearization in balanced distribution system.
Q_{ik0} Initial reactive power of line segment (i,k) for linearization in balanced distribution system.
S_{ik0} Initial apparent power of line segment (i,k) for linearization in balanced distribution system.
V_{i0} Initial voltage of node i for linearization in balanced distribution system.
$\boldsymbol{P}_{ik0}$ Initial active power of line segment (i,k) for linearization in unbalanced distribution system, a 3×1 vector.
$\boldsymbol{Q}_{ik0}$ Initial reactive power of line segment (i,k) for linearization in unbalanced distribution system, a 3×1 vector.
$\mathbf{A}$ A constant real number 3×3 matrix.
$\mathbf{B}$ A constant real number 3×3 matrix.

C. Variables:

S_{ik} Sending end apparent power of line segment (i,k) for balanced distribution system.
$|S_{ik}|$ Mode of S_{ik}.
P_{ik} Sending end active power of line segment (i,k) for balanced distribution system.
Q_{ik} Sending end reactive power of line segment (i,k) for balanced distribution system.
S_k^{d} Apparent power of load at node k for balanced distribution system.
V_k Voltage of node k for balanced distribution system.
$|V_k|$ Mode of V_k.
p_k^{d} Active power of load at node k for balanced distribution system.
q_k^{d} Reactive power of load at node k for balanced distribution system.
U_k Voltage magnitude square of node k for balanced distribution system.
$c_{ik}^{v}(P,Q)$ Square of voltage loss for line segment (i,k) for balanced distribution system.
$c_{ik}^{p}(P,Q)$ Square of active power loss for line segment (i,k) for balanced distribution system.
$c_{ik}^{q}(P,Q)$ Square of reactive power loss for line segment (i,k) for balanced distribution system.
$\boldsymbol{S}_{ik}$ Sending end apparent power of line segment (i,k) for unbalanced distribution system, a 3×1 vector.
$|\boldsymbol{S}_{ik}|$ Mode of $\boldsymbol{S}_{ik}$, a 3×1 vector.
$\boldsymbol{P}_{ik}$ Sending end active power of line segment (i,k) for unbalanced distribution system, a 3×1 vector.
$\boldsymbol{Q}_{ik}$ Sending end reactive power of line segment (i,k) for unbalanced distribution system, a 3×1 vector.
$\boldsymbol{V}_k$ Voltage of node k for unbalanced distribution system, a 3×1 vector.
$|\boldsymbol{V}_k|$ Mode of $\boldsymbol{V}_k$, a 3×1 vector.
$\boldsymbol{U}_k$ Square of voltage magnitude of node k for unbalanced distribution system, a 3×1 vector.
$\boldsymbol{p}_k^{\mathrm{d}}$ Active power of load at node k for unbalanced distribution system, a 3×1 vector.
$\boldsymbol{q}_k^{\mathrm{d}}$ Reactive power of load at node k for unbalanced distribution system, a 3×1 vector.
$\boldsymbol{S}_{ik}^{l}$ Power losses across line segment (i,k) for unbalanced distribution system, a 3×1 vector.
$\boldsymbol{c}_{ik}^{u}(\boldsymbol{P},\boldsymbol{Q})$ Square of voltage loss for line segment (i,k) for unbalanced distribution system, a 3×1 vector.
$\boldsymbol{c}_{ik}^{p}(\boldsymbol{P},\boldsymbol{Q})$ Square of active power loss for line segment (i,k) for unbalanced distribution system, a 3×1 vector.
$\boldsymbol{c}_{ik}^{q}(\boldsymbol{P},\boldsymbol{Q})$ Square of reactive power loss for line segment (i,k) for unbalanced distribution system, a 3×1 vector.
$\rho(t)$ Power price in time interval t.
$P_{\mathrm{EV}k,a,t}$ Charging power of phase a in time interval t for the k^{th} EV with three-phase charging mode.
$P_{\mathrm{EV}k,b,t}$ Charging power of phase b in time interval t for the k^{th} EV with three-phase charging mode.
$P_{\mathrm{EV}k,c,t}$ Charging power of phase c in time interval t for the k^{th} EV with three-phase charging mode.
$P_{\mathrm{EV}k,t}$ Charging power of the k^{th} EV with three-phase charging mode in time interval t.
$P_{\mathrm{EV}m,\beta,t}$ Charging power of the m^{th} EV with single-phase charging mode in time interval t.
$U_{n,\alpha,t}$ Voltage magnitude square of node n phase α in time interval t.
$P_{ik,\alpha,t}$ Power of the line segment (i,k) for phase α in time interval t.
$P_{\mathrm{T},\alpha,t}$ Power of the distribution transformer for phase α in time interval t.
$\boldsymbol{x}$ A 3×1 vector.
$\boldsymbol{y}$ A 3×1 vector.

I. Introduction

WORLDWIDE energy sectors face critical challenges with regard to the security of power supply, environmental impacts, and energy costs. Energy investments are trending towards innovations to improve both the energy efficiency and the environmental friendliness. Compared with traditional vehicles, electric vehicles (EVs) present more significant benefits due to the capability of the non-reliance on oil, reducing harmful gas emissions, and lowering fluctuations of renewable sources. Currently, many countries have accelerated the development of distributed generators (DGs) and EVs. Consequently, some hot research topics come to the fore, including the impact of DGs and EVs on the power system [1]–[3], the optimal operation of distribution networks [4], and the active distribution network technology [5]–[7]. However, the uncoordinated charging of massive EVs could significantly increase network losses, overload distribution transformers or lines, reduce the energy efficiency, and lower system voltages. Whereas smart charging of EVs can significantly improve both economy and reliability benefits of the distribution system.

Generally, researches on the coordinated charging of EVs can be divided into the distributed and centralized methods. The distributed coordinated charging mainly uses the fuzzy mathematics theory [8], sensitivity analysis [9], and iterative method [10]. The centralized coordinated charging generally utilizes the sensitivity analysis [11], [12] and the optimization techniques [13]–[20].

When the objective function is to minimize the total charging costs of holders, distributed EV charging scheduling cannot be applied, because the voltage magnitude and branch power constraints cannot be taken into account. For example, the electricity price is low in peak wind or solar power time and high in peak load time. If a large number of EVs are scattered in different nodes of distribution network, such as EVs in residential distribution network, it is difficult to take voltage magnitude and branch power constraints into account if distributed charging is used to tracking the low electricity price. As a result, safe and economic operation of distribution network cannot be guaranteed. Therefore, centralized coordinated charging is preferable. However, centralized coordinated charging is a large-scale non-linear optimization problem. It is very difficult to solve because of high dimension of optimization variables and large number of constraints. With the popularization of EVs and the progress of battery technology, a large number of EVs will adopt fast charging mode. As a result, optimization time interval must be greatly reduced, and the dimension of optimization variables, number of constraints will increase dramatically. How to improve the computational speed to meet the online rolling optimization requirement is an important topic worthy of study. That is, the computational time is very important in this problem.

In [11], [12], a real-time smart load management strategy is proposed for the coordinated charging of EVs by using the sensitivity analysis technique. However, the control variables are the charging locations rather than the charging power of EVs. It is still challenging to ensure that the EVs can be fully charged. As the coordinated charging of EVs is a large scale optimization problem, many techniques are proposed to improve the computational speed. In [13], a linear constrained convex quadratic programming is formulated to iteratively correct nodal voltages using the power flow calculation. The objective function is to minimize the power losses, while the constraints on voltage magnitudes and thermal loadings of lines/transformers are ignored. However, if the objective function is sensitive to nodal voltages, such as minimizing the total charging costs, the method developed in [13] cannot be applicable.

In [14], [15], with inequality constraints on nodal voltage and thermal loadings of transformers and lines linearized, a LP for the coordinated charging of EVs is proposed to maximize the total charging energy. However, the deviation of linearization of this method is relatively large. Moreover, this method cannot be applicable to the nonlinear objective function, which is not linearly related to the charging power of EVs, such as the minimization of total power supply. In [16], based on Cartesian coordinate power flow equations, a mixed integer LP of coordinated charging of EVs is proposed to maximize the revenue of power corporations with linearized constraints. However, many auxiliary variables and constraints are used to linearize inequality constraints on both the voltage and current, which can significantly increase the complexity of the developed model. Last but not the least, the charging location rather than the charging power is optimized. The formulated mixed integer LP is much more difficult to solve than the LP. In [17], a quadratic programming is proposed to optimize the charging and discharging power of EVs considering the time-of-use power price and battery degradation costs. However, the electricity price is proportional to charging power and other conventional load. In [18], a coordination strategy for optimal charging of EVs is developed by considering the congestion of the distribution system. In [19], a quadratic programming is formulated to minimize the power losses with load balancing. In [20], load factor, load variance, and network losses are demonstrated to be equivalent under certain conditions. As an outcome, minimizing network losses can be transformed to minimizing the load factor or load variance, which can reduce the computational complexity. However, the constraints on nodal voltages or thermal loadings of transformers and lines are not considered in the aforementioned models. When there are massive EVs connected to the distribution system, the constraints on nodal voltages and/or thermal loadings of transformers and lines can be really a factor that limits the charging power of EVs. Though neglecting the constraints on nodal voltages and/or thermal loadings of transformers and lines may significantly improve the computational speed, it may also make the solution to the charging power of EVs unfeasible. When the objective function is to minimize the total charging costs, the constraints on voltages magnitudes and/or thermal loadings of transformers/lines can be a factor that limits the charging power of EVs. As a result, the aforementioned four methods cannot be applicable.

In [21], the influence of charging on the heating and life span of distribution transformer is analyzed. A non-linear model is constructed. However, none of the references [1]–[20] have constructed a non-linear model for transformer heating. Instead, a simple linear inequality with simple branch power or current is formulated. In [22], stochastic analysis is used to analyze the impact of charging randomness on distribution network. At present, for EVCC problem, the rolling optimization is generally used to take into account the uncertainty of EVs and load forecasting.

To cope with the inefficiency of calculation, this paper derives the branch flow equations of balanced and unbalanced distribution system. Moreover, the three-phase imbalance, voltage constraints, and power flow constraints are also considered. The coordinated charging model of EVs is established to minimize total charging costs of holders. The contributions of this paper are as follows. 1) We propose a method to linearize the non-linear terms in branch power flow equations of balanced and unbalanced distribution system and apply it to solve the EVCC problem. As a result, the computing time is greatly reduced. 2) The conventional load in branch power flow equations includes constant impedance and constant power load. 3) We have proposed how to compute the initial point of linearization. 4) The capabilities of the proposed method-fast calculation speed and high accuracy are

verified by four simulation cases and compared with recent similar work.

The organization of this paper is as follows. Branch flow equations of balanced and unbalanced distribution systems are introduced in Section II. The coordinated charging model of EVs is formulated in Section III-C. A fast solving method is described in Section V. Both the accuracy and computational efficiency of the developed method are discussed in Section VI. Section VII concludes the paper.

II. EVCC Problem

The EVCC problem is to determine an EV battery charging schedule so that distribution system operates with optimal cost and satisfies operational constraints. In this paper, the following descriptions are assumed [16].

1) The EV batteries must be charged in a given period of time, which is divided into several time intervals.

2) The energy required by each battery is known at the beginning of the time period.

3) The EVs have communication devices that allow the distribution system operator to control the charging power of the batteries. That control can be carried out in each time interval of the time period.

Operational constraints, such as voltage magnitude limits, power generation limits, and maximum circuit power must be satisfied. The optimal charging schedule defines the charging power of each EV battery in each time interval. The estimated arrival and departure times for the EVs are considered using parameters t_{ks} and t_{ke}, respectively. These parameters, as well as the initial charge state of a battery (E_k^{ini}), can be obtained using estimation techniques applied to EVs, such as those in [23]–[25]. The mathematical model considers these parameters, allowing the EV to be charged only during the time interval between arrival and departure.

III. NLP model for the EVCC problem

A. Branch Flow Equations in Balanced Distribution Systems

The distribution system with symmetrical parameters is referred as balanced distribution system while that with three-phase conductors not transposed or with large load differences among three-phase is referred as unbalanced distribution system. Balanced distribution system can be represented by single-phase model while unbalanced distribution system must be represented by a three-phase model.

To improve the computational speed, models of the three-phase balance and unbalanced distribution systems are constructed by using branch flow equations. Given an $N+1$ bus distribution system with a tree topology, i.e., a radial network without loops between branches, the root bus is denoted by $N+1$ and the remaining N buses of the system are denoted by the set $\mathbb{N} = \{1, 2, \cdots, N\}$. The edge-set that represents the set of distribution line segments (including conductors for single-, two-, and three-phase circuits) is denoted by $\varepsilon \subseteq \{\mathbb{N} \cup \{N+1\}\} \times \{\mathbb{N} \cup \{N+1\}\}$ with $(i,k) \in \varepsilon$, if there is a distribution line segment between bus i and bus k (bus i closer to the feeder). Note that all the edges are directed so that we can get $(i,k) \in \varepsilon \Rightarrow (k,i) \notin \varepsilon$. The Π type equivalent

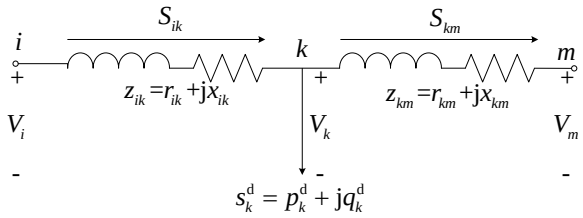

Fig. 1. Branch flow of distribution systems.

circuit is used to represent the line segments. The impedance of the line segment (i,k) is given by $z_{ik} = r_{ik} + \mathrm{j}x_{ik}$. The demand at bus k considering the shunt capacitance of the line is denoted by $s_k^{\mathrm{d}} = p_k^{\mathrm{d}} + \mathrm{j}q_k^{\mathrm{d}}$. Considering the circuit shown in Fig. 1, both the voltage drop and power flow equations are formulated by using the notation and orientation.

Let $H_k = \{j \,|(k,j) \in \varepsilon\}$ be the set of buses downstream of bus k. The total power flow $S_{ik} \in \mathbb{C}$ transferred through the sending end of distribution line segment (i,k) is given by:

$$S_{ik} = \sum_{j \in H_k} S_{kj} + S_k^{\mathrm{d}} + z_{ik} \frac{|S_{ik}|^2}{|V_i|^2} \tag{1}$$

where the line power flow S_{ik} is always relative to the sending end voltage, $V_i = |V_i| \angle \theta_i$, of the distribution line segment. The voltage of bus k based on the upstream bus i is given by:

$$V_k = V_i - z_{ik} \frac{P_{ik} - jQ_{ik}}{V_i^*} \tag{2}$$

where the root node voltage is fixed with $V_{N+1} = V^s = |V^s| \angle 0$ for a constant $|V^s|$. The dependence on the phase angles in (2) is removed by taking the product of each side of (2) with its conjugate. Thus, the branch flow equations for an $N+1$ bus network is given by:

$$V_{N+1} = V^s = |V^s| \angle 0 \tag{3a}$$

$$|V_k|^2 = |V_i|^2 - 2\left(r_{ik}P_{ik} + x_{ik}Q_{ik}\right) + |z_{ik}|^2 \frac{|S_{ik}|^2}{|V_i|^2} \tag{3b}$$

$$P_{ik} = \sum_{j \in H_k} P_{kj} + p_k^{\mathrm{d}} + r_{ik} \frac{|S_{ik}|^2}{|V_i|^2} \tag{3c}$$

$$Q_{ik} = \sum_{j \in H_k} Q_{kj} + q_k^{\mathrm{d}} + x_{ik} \frac{|S_{ik}|^2}{|V_i|^2} \tag{3d}$$

The power demand is usually a mix of constant power and constant impedance load. Thus, it can be expressed as:

$$p_k^{\mathrm{d}} = p_{k0}^{\mathrm{d}} + p_{kz0}^{\mathrm{d}} |V_k|^2 \tag{4a}$$

$$q_k^{\mathrm{d}} = q_{k0}^{\mathrm{d}} + q_{kz0}^{\mathrm{d}} |V_k|^2 \tag{4b}$$

According to (3)–(4) and given $U_i = |V_i|^2$, the branch flow equations of the three-phase balanced distribution system can

be simplified as:

$$U_{N+1} = |V^s|^2 = U^s \tag{5a}$$

$$U_k = U_i - 2\left(r_{ik}P_{ik} + x_{ik}Q_{ik}\right) + c_{ik}^{v}\left(P,Q\right),\ k \in \mathbb{N} \tag{5b}$$

$$P_{ik} = \sum_{j \in H_k} P_{kj} + p_k^{\mathrm{d}} + c_{ik}^{p}\left(P,Q\right),\ k \in \mathbb{N} \tag{5c}$$

$$Q_{ik} = \sum_{j \in H_k} Q_{kj} + q_k^{\mathrm{d}} + c_{ik}^{q}\left(P,Q\right),\ k \in \mathbb{N} \tag{5d}$$

$$p_k^{\mathrm{d}} = p_{k0}^{\mathrm{d}} + p_{kz0}^{\mathrm{d}} U_k,\ k \in \mathbb{N} \tag{5e}$$

$$q_k^{\mathrm{d}} = q_{k0}^{\mathrm{d}} + q_{kz0}^{\mathrm{d}} U_k,\ k \in \mathbb{N} \tag{5f}$$

where $c_{ik}^{v}\left(P,Q\right) = |z_{ik}|^2|S_{ik}|^2\Big/|V_i|^2$, $c_{ik}^{p}\left(P,Q\right) = r_{ik}|S_{ik}|^2\Big/|V_i|^2$, and $c_{ik}^{q}\left(P,Q\right) = x_{ik}|S_{ik}|^2\Big/|V_i|^2$.

B. Branch Flow in Unbalanced Distribution Systems

In the actual distribution system, the overhead lines are usually not transposed. Thus, the off diagonal elements of the line mutual impedance matrix are not equal any more. Moreover, the three-phase loads connected to each node are usually not equal. As a result, the three-phase parameters of the distribution system are asymmetrical. For each line segment $(i,k) \in \varepsilon$, the voltage equation is given by:

$$\boldsymbol{V}_k = \boldsymbol{V}_i - \boldsymbol{z}_{ik}\left[\left(\boldsymbol{P}_{ik} - \mathrm{j}\boldsymbol{Q}_{ik}\right) \varnothing \boldsymbol{V}_i^*\right] \tag{6}$$

where $\boldsymbol{z}_{ik} \in \mathbb{C}^{3\times3}$, $\boldsymbol{V}_k = [V_{ka}, V_{kb}, V_{kc}]^{\mathrm{T}}$, $\boldsymbol{V}_i = [V_{ia}, V_{ib}, V_{ic}]^{\mathrm{T}}$, $\boldsymbol{P}_{ik} = [P_{ika}, P_{ikb}, P_{ikc}]^{\mathrm{T}}$, and $\boldsymbol{Q}_{ik} = [Q_{ika}, Q_{ikb}, Q_{ikc}]^{\mathrm{T}}$. The symbol of $\varnothing$ denotes the element-wise division.

Unlike the per-phase equivalent case, both sides of (6) cannot remove the dependence on phase angles by multiplying the complex conjugate. This is due to the fact that there is a coupling between phases that arises from the cross-product of the three-phase equation for the phase voltage and line current. To address this problem, it can be observed that voltage magnitudes between phases are similar, i.e., $|V_{ia}| \approx |V_{ib}| \approx |V_{ic}|$ [26] and the unbalance on each phase are not that severe. Thus, voltage magnitudes are assumed to be approximately equal. The unbalance of the three-phase angle α is relatively small (typically within $1^\circ \sim 3^\circ$). Thus, we ignore α and assume that the three-phase voltage at each node is equal. By multiplying both sides of (6) with its conjugate vector, the voltage equation in (5b) can be updated as:

$$|\boldsymbol{V}_k|^2 = |\boldsymbol{V}_i|^2 - 2\left(\tilde{\boldsymbol{r}}_{ik}\mathbf{P}_{ik} + \tilde{\boldsymbol{x}}_{ik}\mathbf{Q}_{ik}\right) + \boldsymbol{c}_{ik}^{u}\left(\boldsymbol{P},\boldsymbol{Q}\right),\ k \in \mathbb{N} \tag{7}$$

$$\mathbf{a} = \begin{bmatrix} 1 & e^{-\mathrm{j}2\pi/3} & e^{\mathrm{j}2\pi/3} \end{bmatrix}^{\mathrm{T}} \tag{8}$$

$$\tilde{\boldsymbol{r}}_{ik} = \mathrm{Re}\left\{\mathbf{a}\mathbf{a}^{\mathrm{H}}\right\} \odot \boldsymbol{r}_{ik} + \mathrm{Im}\left\{\mathbf{a}\mathbf{a}^{\mathrm{H}}\right\} \odot \boldsymbol{x}_{ik} \tag{9}$$

$$\tilde{\boldsymbol{x}}_{ik} = \mathrm{Re}\left\{\mathbf{a}\mathbf{a}^{\mathrm{H}}\right\} \odot \boldsymbol{x}_{ik} - \mathrm{Im}\left\{\mathbf{a}\mathbf{a}^{\mathrm{H}}\right\} \odot \boldsymbol{r}_{ik} \tag{10}$$

$$\boldsymbol{c}_{ik}^{u}\left(\boldsymbol{P},\boldsymbol{Q}\right) = \left[\boldsymbol{z}_{ik}\left(\boldsymbol{S}_{ik}^* \varnothing \boldsymbol{V}_i^*\right)\right] \odot \left[\boldsymbol{z}_{ik}^*\left(\boldsymbol{S}_{ik} \varnothing \boldsymbol{V}_i\right)\right] \tag{11}$$

where the symbol of $\odot$ denotes the element-wise multiplication.

We assume that the three-phase voltages magnitudes of each node are equal in order to obtain a constant equivalent resistance matrix $\tilde{\boldsymbol{r}}_{ik}$ and reactance matrix $\tilde{\boldsymbol{x}}_{ik}$, thus simplifying the voltage equation. This hypothesis is only used to derive Eq. (7) and is not used for other purposes. Eq. (7) shows that when the three-phase power of each branch is unequal, the three-phase voltages magnitudes of each node are unequal as well. Thus, Eq. (7) simulates the three-phase unbalanced distribution network. Eq. (7) has high accuracy, because the unbalance of three-phase voltage of each node in the actual distribution network is very small. The voltage imbalance limit in the distribution system is that the negative sequence voltage divided by the positive sequence voltage must be below 2% which is required by the National Electrical Manufacturers Association (NEMA). In the actual distribution network, the imbalance of three-phase voltage is very small while the imbalance of three-phase power may be large.

Branch flow equations in (5c) and (5d) can be updated as:

$$\boldsymbol{P}_{ik} = \sum_{j \in H_k} \boldsymbol{P}_{kj} + \boldsymbol{p}_k^{\mathrm{d}} + \boldsymbol{c}_{ik}^{p}\left(\boldsymbol{P},\boldsymbol{Q}\right),\ k \in \mathbb{N} \tag{12}$$

$$\boldsymbol{Q}_{ik} = \sum_{j \in H_k} \boldsymbol{Q}_{kj} + \boldsymbol{q}_k^{\mathrm{d}} + \boldsymbol{c}_{ik}^{q}\left(\boldsymbol{P},\boldsymbol{Q}\right),\ k \in \mathbb{N} \tag{13}$$

where $\boldsymbol{c}_{ik}^{p}\left(\boldsymbol{P},\boldsymbol{Q}\right) = \mathrm{Re}\left\{\left(\boldsymbol{S}_{ik} \varnothing \boldsymbol{V}_i\right) \odot \left(\boldsymbol{V}_i - \boldsymbol{V}_k\right)\right\}$, $\boldsymbol{c}_{ik}^{q}\left(\boldsymbol{P},\boldsymbol{Q}\right) = \mathrm{Im}\left\{\left(\boldsymbol{S}_{ik} \varnothing \boldsymbol{V}_i\right) \odot \left(\boldsymbol{V}_i - \boldsymbol{V}_k\right)\right\}$

Power demand equations in (5e) and (5f) can be updated as:

$$\boldsymbol{p}_k^{\mathrm{d}} = \boldsymbol{p}_{k0}^{\mathrm{d}} + \boldsymbol{p}_{kz0}^{\mathrm{d}} \boldsymbol{U}_k,\ k \in \mathbb{N} \tag{14}$$

$$\boldsymbol{q}_k^{\mathrm{d}} = \boldsymbol{q}_{k0}^{\mathrm{d}} + \boldsymbol{q}_{kz0}^{\mathrm{d}} \boldsymbol{U}_k,\ k \in \mathbb{N} \tag{15}$$

The three-phase voltage of the root node in (5a) is updated as:

$$\boldsymbol{U}_{N+1} = |\boldsymbol{V}^s| \odot |\boldsymbol{V}^s| \tag{16}$$

C. Model for EVCC

The objective function for the coordinated charging model of EVs is to minimize the total charging costs of holders, given by:

$$J = \min \sum_{t=t_1}^{t_{\max}} \rho\left(t\right) \left(\sum_{k=1}^{K} P_{\mathrm{EV}k,t} + \sum_{m=1}^{M} P_{\mathrm{EV}m,\beta,t} \right) \Delta t \tag{17}$$

Constraints on the charging power of each EV with the three-phase charging mode are formulated by:

$$0 \le P_{\mathrm{EV}k,t} \le P_{\mathrm{EV}k,\max} \tag{18}$$

$$P_{\mathrm{EV}k,a,t} = P_{\mathrm{EV}k,b,t} = P_{\mathrm{EV}k,c,t} = \frac{P_{\mathrm{EV}k,t}}{3} \tag{19}$$

The constraint on the charging power of each EV with the single-phase charging mode is formulated by:

$$0 \le P_{\mathrm{EV}m,\beta,t} \le P_{\mathrm{EV}m,\max} \tag{20}$$

Constraints on the power demand of each EV with the three- and single-phase charging modes are given by:

$$\eta \sum_{t=t_{ks}}^{t_{ke}} P_{\mathrm{EV}k,t} \Delta t = E_k^{\mathrm{cap}} - E_k^{\mathrm{ini}} \tag{21}$$

$$\eta \sum_{t=t_{ms}}^{t_{me}} P_{\mathrm{EV}m,\beta,t} \Delta t = E_m^{\mathrm{cap}} - E_m^{\mathrm{ini}} \tag{22}$$

The rates of charging power constraints are considered in Eqs. (18)–(20), while the SOC constraints are indirectly considered in Eqs. (21) and (22). The discharging mode (Vehicle to Grid) can be added to this work as well. To do this, it is only needed to modify Eqs. (18)–(22). However, since the discharging mode can reduce the battery life span, it is not considered in this paper.

The constraint on the nodal voltage of the distribution system is given by:

$$U_{\min} \le U_{n,\alpha,t} \le U_{\max} \tag{23}$$

The constraint on the thermal loading of each line is given by:

$$0 \le P_{ik,\alpha,t} \le P_{ik,\alpha,t}^{\max} \tag{24}$$

The constraint on the thermal loading of each transformer is given by:

$$0 \le P_{\mathrm{T},\alpha,t} \le P_{\mathrm{T},\alpha,t}^{\max} \tag{25}$$

For the balanced distribution system, the objective function is formulated in (17). Equality constraints are formulated in (5a)–(5f), (19), and (21). Inequality constraints are formulated in (20) and (23)–(25). For the unbalanced distribution system, the objective function is formulated in (17). Equality constraints are formulated in (7), (12)–(16), (19), and (21)–(22). Inequality constraints are formulated in (18), (20) and (23)–(25).

The charging power of EVs is constrained by the voltage magnitude and branch power. For different distribution network models, the function relationship between the voltage magnitude, branch power, and charging power is different, which leads to different objective function values, i.e., total charging costs of holders. If the distribution network is balanced and all EVs are charged with the three–phase mode, the balanced distribution network model can be used. Otherwise, the unbalanced distribution network model must be adopted.

IV. LP Model for the EVCC Problem

In the formulated NLP EVCC problem, only the model of distribution network is nonlinear, while other parts are linear. We propose a method to linearize the model of balanced and unbalanced distribution network. However, for the charge scheduling problem, the initial point of linearizing is unknown in advance. We propose a method to calculate the initial point of linearizing. The linearizing process is closely associated with the charging scheduling model.

The advantage of LP is that it can be solved quickly by using sophisticated solver. A mixed-integer LP is formulated in [16]. However, polar coordinate power flow equations are adopted. While in our paper, branch power flow equations are utilized. The variable number is much less than that in [16]. Further, non-linear inequalities are linearized by introducing new auxiliary variables in [16]. As a result, variables have sharply increased. While in our paper, we linearize the non-linear terms in branch power flow equations by using Taylor expansion and the variable number keeps constant.

A. Linearization of Branch Flow Equations in the Balanced Distribution System

In (5a)–(5f), only $c_{ik}^{v}(P,Q)$, $c_{ik}^{p}(P,Q)$, and $c_{ik}^{q}(P,Q)$ are nonlinear terms. To fast solve the developed model, it should be linearized. Let:

$$h_{ik}(P,Q) = \frac{|S_{ik}|^2}{|V_i|^2} = \frac{P_{ik}^2 + Q_{ik}^2}{|V_i|^2} \tag{26}$$

$$c_{ik}^{v}(P,Q) = |z_{ik}|^2 h_{ik}(P,Q) \tag{27a}$$

$$c_{ik}^{p}(P,Q) = r_{ik} h_{ik}(P,Q) \tag{27b}$$

$$c_{ik}^{q}(P,Q) = x_{ik} h_{ik}(P,Q) \tag{27c}$$

$h_{ik}(P,Q)$ can be linearized as:

$$h_{ik}(P,Q) \approx \frac{2P_{ik0}P_{ik} + 2Q_{ik0}Q_{ik} - |S_{ik0}|^2}{|V_{i0}|^2} \tag{28}$$

B. Linearization of Branch flow Equations in the Unbalanced Distribution System

1) Linearization of the Nonlinear Term in Voltage Equations: Let $\bar{\boldsymbol{a}}_i = \left[1, e^{\mathrm{j}2\pi/3} e^{-\mathrm{j}2\pi/3}\right]^{\mathrm{T}} \oslash |\boldsymbol{V}_i|$, then the nonlinear term of the voltage equation can be expressed as:

$$\begin{aligned} \boldsymbol{c}_{ik}^{u}(\boldsymbol{P},\boldsymbol{Q}) &= [\boldsymbol{z}_{ik}(\boldsymbol{S}_{ik}^{*} \oslash \boldsymbol{V}_i^{*})] \odot [\boldsymbol{z}_{ik}^{*}(\boldsymbol{S}_{ik} \oslash \boldsymbol{V}_i)] \\ &\approx [\boldsymbol{z}_{ik}(\boldsymbol{S}_{ik}^{*} \odot \bar{\boldsymbol{a}}_i^{*})] \odot [\boldsymbol{z}_{ik}^{*}(\boldsymbol{S}_{ik} \odot \bar{\boldsymbol{a}}_i)] \end{aligned} \tag{29}$$

A new branch impedance matrix is defined as:

$$\bar{\boldsymbol{z}}_{ik} = \boldsymbol{z}_{ik} diag(\bar{\boldsymbol{a}}_i^{*}) = \bar{\boldsymbol{r}}_{ik} + \mathrm{j}\bar{\boldsymbol{x}}_{ik} \tag{30}$$

Then, (29) can be rewritten as:

$$\begin{aligned} \boldsymbol{c}_{ik}^{u}(\boldsymbol{P},\boldsymbol{Q}) = {} & (\bar{\boldsymbol{r}}_{ik}\boldsymbol{P}_{ik}) \odot (\bar{\boldsymbol{r}}_{ik}\boldsymbol{P}_{ik}) + (\bar{\boldsymbol{x}}_{ik}\boldsymbol{Q}_{ik}) \odot (\bar{\boldsymbol{x}}_{ik}\boldsymbol{Q}_{ik}) \\ & + (\bar{\boldsymbol{x}}_{ik}\boldsymbol{P}_{ik}) \odot (\bar{\boldsymbol{x}}_{ik}\boldsymbol{P}_{ik}) + (\bar{\boldsymbol{r}}_{ik}\boldsymbol{Q}_{ik}) \odot (\bar{\boldsymbol{r}}_{ik}\boldsymbol{Q}_{ik}) \\ & + 2(\bar{\boldsymbol{r}}_{ik}\boldsymbol{P}_{ik}) \odot (\bar{\boldsymbol{x}}_{ik}\boldsymbol{Q}_{ik}) - 2(\bar{\boldsymbol{x}}_{ik}\boldsymbol{P}_{ik}) \odot (\bar{\boldsymbol{r}}_{ik}\boldsymbol{Q}_{ik}) \end{aligned} \tag{31}$$

The linearization of $\boldsymbol{c}_{ik}^{u}(\boldsymbol{P},\boldsymbol{Q})$ is defined as:

$$\begin{aligned} \boldsymbol{c}_{ik}^{u}(\boldsymbol{P},\boldsymbol{Q}) \approx {} & \boldsymbol{u}_{pik}(\boldsymbol{P}_{ik0},\boldsymbol{Q}_{ik0})(\boldsymbol{P}_{ik} - \boldsymbol{P}_{ik0}) \\ & + \boldsymbol{u}_{qik}(\boldsymbol{P}_{ik0},\boldsymbol{Q}_{ik0})(\boldsymbol{Q}_{ik} - \boldsymbol{Q}_{ik0}) + \boldsymbol{c}_{ik}^{u}(\boldsymbol{P}_{ik0},\boldsymbol{Q}_{ik0}) \end{aligned} \tag{32}$$

According to (31), the partial derivatives are given by:

$$\begin{aligned} \boldsymbol{u}_{pik} = \frac{\partial \boldsymbol{c}_{ik}^{u}}{\partial \boldsymbol{P}_{ik}} = {} & \boldsymbol{h}_{xx}(\bar{\boldsymbol{r}}_{ik},\boldsymbol{P}_{ik}) + \boldsymbol{h}_{xx}(\bar{\boldsymbol{x}}_{ik},\boldsymbol{P}_{ik}) \\ & + 2\boldsymbol{h}_{xy}(\bar{\boldsymbol{r}}_{ik},\bar{\boldsymbol{x}}_{ik},\boldsymbol{P}_{ik},\boldsymbol{Q}_{ik}) \\ & - 2\boldsymbol{h}_{xy}(\bar{\boldsymbol{x}}_{ik},\bar{\boldsymbol{r}}_{ik},\boldsymbol{P}_{ik},\boldsymbol{Q}_{ik}) \end{aligned} \tag{33}$$

$$\begin{aligned} \boldsymbol{u}_{qik} = \frac{\partial \boldsymbol{c}_{ik}^{u}}{\partial \boldsymbol{Q}_{ik}} = {} & \boldsymbol{h}_{xx}(\bar{\boldsymbol{r}}_{ik},\boldsymbol{Q}_{ik}) + \boldsymbol{h}_{xx}(\bar{\boldsymbol{x}}_{ik},\boldsymbol{Q}_{ik}) \\ & + 2\boldsymbol{h}_{xy}(\bar{\boldsymbol{x}}_{ik},\bar{\boldsymbol{r}}_{ik},\boldsymbol{Q}_{ik},\boldsymbol{P}_{ik}) \\ & - 2\boldsymbol{h}_{xy}(\bar{\boldsymbol{r}}_{ik},\bar{\boldsymbol{x}}_{ik},\boldsymbol{Q}_{ik},\boldsymbol{P}_{ik}) \end{aligned} \tag{34}$$

where functions $\boldsymbol{h}_{xx}$ and $\boldsymbol{h}_{xy}$ are respectively given by:

$$\boldsymbol{h}_{xx}\left(\mathbf{A},\boldsymbol{x}\right)=2diag\left(\mathbf{A}\boldsymbol{x}\right)\mathbf{A} \tag{35}$$

$$\boldsymbol{h}_{xy}\left(\mathbf{A},\mathbf{B},\boldsymbol{x},\boldsymbol{y}\right)=diag\left(\mathbf{B}\boldsymbol{y}\right)\mathbf{A} \tag{36}$$

2) Linearization of the Nonlinear Term in Power Equations: The power loss across line segment (i,k) is given by:

$$\boldsymbol{S}_{ik}^{l}=\left(\boldsymbol{S}_{ik}\varnothing\boldsymbol{V}_{i}\right)\odot\left[\boldsymbol{z}_{ik}\left(\boldsymbol{S}_{ik}^{*}\varnothing\boldsymbol{V}_{i}^{*}\right)\right] \tag{37}$$

Another branch impedance matrix is redefined as:

$$\hat{\boldsymbol{z}}_{ik}=\hat{\boldsymbol{r}}_{ik}+\mathrm{j}\hat{\boldsymbol{x}}_{ik}=\boldsymbol{z}_{ik}\odot\left(\bar{\boldsymbol{a}}_{i}\bar{\boldsymbol{a}}_{i}^{\mathrm{H}}\right) \tag{38}$$

According to (38), by separating the real part from the imaginary one, it can be obtained:

$$\hat{\boldsymbol{r}}_{ik}=\mathrm{Re}\left\{\bar{\boldsymbol{a}}_{i}\bar{\boldsymbol{a}}_{i}^{\mathrm{H}}\right\}\odot\boldsymbol{r}_{ik}-\mathrm{Im}\left\{\bar{\boldsymbol{a}}_{i}\bar{\boldsymbol{a}}_{i}^{\mathrm{H}}\right\}\odot\boldsymbol{x}_{ik} \tag{39}$$

$$\hat{\boldsymbol{x}}_{ik}=\mathrm{Re}\left\{\bar{\boldsymbol{a}}_{i}\bar{\boldsymbol{a}}_{i}^{\mathrm{H}}\right\}\odot\boldsymbol{x}_{ik}+\mathrm{Im}\left\{\bar{\boldsymbol{a}}_{i}\bar{\boldsymbol{a}}_{i}^{\mathrm{H}}\right\}\odot\boldsymbol{r}_{ik} \tag{40}$$

For the sake of simplicity, (37) can be rewritten as:

$$\boldsymbol{S}_{ik}^{l}=\left(\boldsymbol{P}_{ik}+\mathrm{j}\boldsymbol{Q}_{ik}\right)\odot\left[\hat{\boldsymbol{z}}_{ik}\left(\boldsymbol{P}_{ik}-\mathrm{j}\boldsymbol{Q}_{ik}\right)\right] \tag{41}$$

According to (39)–(41), by separating the active power from the reactive power, it can be obtained:

$$\begin{aligned}\boldsymbol{c}_{ik}^{p}\left(\boldsymbol{P},\boldsymbol{Q}\right)=\mathrm{real}\left(\boldsymbol{S}_{ik}^{l}\right)&=\boldsymbol{P}_{ik}\odot\left(\hat{\boldsymbol{r}}_{ik}\boldsymbol{P}_{ik}+\hat{\boldsymbol{x}}_{ik}\boldsymbol{Q}_{ik}\right)\\&+\boldsymbol{Q}_{ik}\odot\left(\hat{\boldsymbol{r}}_{ik}\boldsymbol{Q}_{ik}-\hat{\boldsymbol{x}}_{ik}\boldsymbol{P}_{ik}\right)\end{aligned} \tag{42}$$

$$\begin{aligned}\boldsymbol{c}_{ik}^{q}\left(\boldsymbol{P},\boldsymbol{Q}\right)=\mathrm{imag}\left(\boldsymbol{S}_{ik}^{l}\right)&=\boldsymbol{P}_{ik}\odot\left(\hat{\boldsymbol{x}}_{ik}\boldsymbol{P}_{ik}-\hat{\boldsymbol{r}}_{ik}\boldsymbol{Q}_{ik}\right)\\&+\boldsymbol{Q}_{ik}\odot\left(\hat{\boldsymbol{r}}_{ik}\boldsymbol{P}_{ik}+\hat{\boldsymbol{x}}_{ik}\boldsymbol{Q}_{ik}\right)\end{aligned} \tag{43}$$

The linearization of $\boldsymbol{c}_{ik}^{p}\left(\boldsymbol{P},\boldsymbol{Q}\right)$ and $\boldsymbol{c}_{ik}^{q}\left(\boldsymbol{P},\boldsymbol{Q}\right)$ are respectively defined as:

$$\begin{aligned}\boldsymbol{c}_{ik}^{p}\left(\boldsymbol{P},\boldsymbol{Q}\right)\approx&\boldsymbol{f}_{pik}\left(\boldsymbol{P}_{ik0},\boldsymbol{Q}_{ik0}\right)\left(\boldsymbol{P}_{ik}-\boldsymbol{P}_{ik0}\right)\\&+\boldsymbol{f}_{qik}\left(\boldsymbol{P}_{ik0},\boldsymbol{Q}_{ik0}\right)\left(\boldsymbol{Q}_{ik}-\boldsymbol{Q}_{ik0}\right)+\boldsymbol{c}_{ik}^{p}\left(\boldsymbol{P}_{ik0},\boldsymbol{Q}_{ik0}\right)\end{aligned} \tag{44}$$

$$\begin{aligned}\boldsymbol{c}_{ik}^{q}\left(\boldsymbol{P},\boldsymbol{Q}\right)\approx&\boldsymbol{g}_{pik}\left(\boldsymbol{P}_{ik0},\boldsymbol{Q}_{ik0}\right)\left(\boldsymbol{P}_{ik}-\boldsymbol{P}_{ik0}\right)\\&+\boldsymbol{g}_{qik}\left(\boldsymbol{P}_{ik0},\boldsymbol{Q}_{ik0}\right)\left(\boldsymbol{Q}_{ik}-\boldsymbol{Q}_{ik0}\right)+\boldsymbol{c}_{ik}^{q}\left(\boldsymbol{P}_{ik0},\boldsymbol{Q}_{ik0}\right)\end{aligned} \tag{45}$$

Partial derivative terms in (44) and (45) are respectively given by:

$$\begin{aligned}\boldsymbol{f}_{pik}=\frac{\partial\boldsymbol{c}_{ik}^{p}}{\partial\boldsymbol{P}_{ik}}&=\tilde{\boldsymbol{h}}_{xx}\left(\hat{\boldsymbol{r}}_{ik},\boldsymbol{P}_{ik}\right)+\tilde{\boldsymbol{h}}_{xy}\left(\hat{\boldsymbol{x}}_{ik},\boldsymbol{P}_{ik},\boldsymbol{Q}_{ik}\right)\\&-\tilde{\boldsymbol{h}}_{yx}\left(\hat{\boldsymbol{x}}_{ik},\boldsymbol{Q}_{ik},\boldsymbol{P}_{ik}\right)\end{aligned} \tag{46}$$

$$\begin{aligned}\boldsymbol{f}_{qik}=\frac{\partial\boldsymbol{c}_{ik}^{p}}{\partial\boldsymbol{Q}_{ik}}&=\tilde{\boldsymbol{h}}_{xx}\left(\hat{\boldsymbol{r}}_{ik},\boldsymbol{Q}_{ik}\right)-\tilde{\boldsymbol{h}}_{xy}\left(\hat{\boldsymbol{x}}_{ik},\boldsymbol{Q}_{ik},\boldsymbol{P}_{ik}\right)\\&+\tilde{\boldsymbol{h}}_{xy}\left(\hat{\boldsymbol{x}}_{ik},\boldsymbol{P}_{ik},\boldsymbol{Q}_{ik}\right)\end{aligned} \tag{47}$$

$$\begin{aligned}\boldsymbol{g}_{pik}=\frac{\partial\boldsymbol{c}_{ik}^{q}}{\partial\boldsymbol{P}_{ik}}&=\tilde{\boldsymbol{h}}_{xx}\left(\hat{\boldsymbol{x}}_{ik},\boldsymbol{P}_{ik}\right)-\tilde{\boldsymbol{h}}_{xy}\left(\hat{\boldsymbol{r}}_{ik},\boldsymbol{P}_{ik},\boldsymbol{Q}_{ik}\right)\\&+\tilde{\boldsymbol{h}}_{yx}\left(\hat{\boldsymbol{r}}_{ik},\boldsymbol{Q}_{ik},\boldsymbol{P}_{ik}\right)\end{aligned} \tag{48}$$

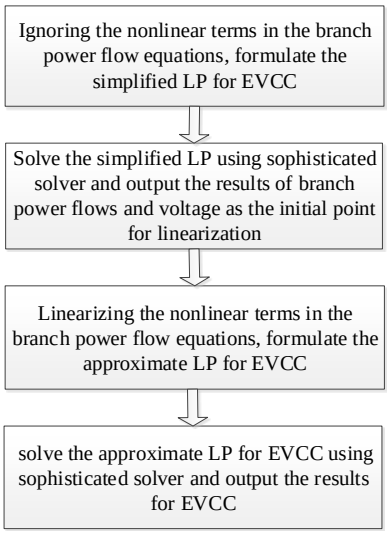

Fig. 2. Schematic of the proposed fast solving method.

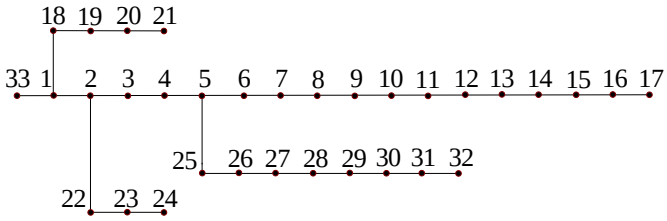

Fig. 3. IEEE 33-node distribution system.

$$\begin{aligned}\boldsymbol{g}_{qik}=\frac{\partial\boldsymbol{c}_{ik}^{q}}{\partial\boldsymbol{Q}_{ik}}&=\tilde{\boldsymbol{h}}_{xx}\left(\hat{\boldsymbol{x}}_{ik},\boldsymbol{Q}_{ik}\right)+\tilde{\boldsymbol{h}}_{xy}\left(\hat{\boldsymbol{r}}_{ik},\boldsymbol{Q}_{ik},\boldsymbol{P}_{ik}\right)\\&-\tilde{\boldsymbol{h}}_{yx}\left(\hat{\boldsymbol{r}}_{ik},\boldsymbol{P}_{ik},\boldsymbol{Q}_{ik}\right)\end{aligned} \tag{49}$$

where functions $\tilde{\boldsymbol{h}}_{xx}$, $\tilde{\boldsymbol{h}}_{xy}$, and $\tilde{\boldsymbol{h}}_{yx}$ are respectively given by:

$$\tilde{\boldsymbol{h}}_{xx}\left(\mathbf{A},\boldsymbol{x}\right)=diag\left(\mathbf{A}\boldsymbol{x}\right)+diag\left(\boldsymbol{x}\right)\mathbf{A} \tag{50}$$

$$\tilde{\boldsymbol{h}}_{xy}\left(\mathbf{A},\boldsymbol{x},\boldsymbol{y}\right)=diag\left(\mathbf{A}\boldsymbol{y}\right) \tag{51}$$

$$\tilde{\boldsymbol{h}}_{yx}\left(\mathbf{A},\boldsymbol{y},\boldsymbol{x}\right)=diag\left(\boldsymbol{y}\right)\mathbf{A} \tag{52}$$

V. Fast Solving Method

The accuracy of linearization is closely associated with the initial point. However, it is challenging to know the initial point since it is not the actual operation point. Toward this end, the nonlinear terms of the voltage $\boldsymbol{c}_{ik}^{u}\left(\boldsymbol{P},\boldsymbol{Q}\right)$, active power $\boldsymbol{c}_{ik}^{p}\left(\boldsymbol{P},\boldsymbol{Q}\right)$, and reactive power $\boldsymbol{c}_{ik}^{q}\left(\boldsymbol{P},\boldsymbol{Q}\right)$ are first ignored. The simplified LP for coordinated charging of EVs is formulated. Then, the sophisticated LP solver is used to solve this simplified LP. The output is taken as the initial point of linearization. Whereafter, the approximated LP for coordinated charging of EVs is formulated. Finally, the sophisticated LP solver is used to solve this approximated LP once again and output the optimal charging power of EVs. Losses of the voltage, active power, and reactive power are

much less than the corresponding linear terms in branch flow equations. In addition, the linearization is performed at the initial point that is the result of the simplified linear model. Thus, the deviation is relatively small. That is, the accuracy of the proposed linearization strategy can be guaranteed. The computational speed of the proposed method can also be guaranteed since both formulated models belong to the LP problem. A schematic diagram of the proposed fast solving method is shown in Fig. 2.

VI. Case Studies

In the simulation cases, noon or night are chosen as the charging periods since these time periods are in coincidence with the charging habits of most EV holders.

A. Case 1

1) Simulation Conditions: Fig. 3 shows the IEEE 33-node medium voltage (MV) distribution system to test the capability of the proposed method. The impedance matrix of transmission lines is shown in Table I. In this system, node 33 is taken as the slack node and its voltage is kept to be 1.00 p.u.. The rest of nodes are taken as PQ nodes. The base conventional load at each node is shown in Table II. The constant power load model is deployed. There are four parking lots of EVs connected at nodes 17, 21, 24, and 32, respectively. There are 40 EVs in each parking lot. The single-phase base power and voltage are chosen to be $1000/3$ kVA and $12.66/\sqrt{3}$ kV, respectively. The back forward sweep method is used to calculate the power flow.

Other simulation conditions are set as follows:

1) All EV owners are willing to participate in the coordinated charging. The charging power of each EV is fully controllable. The charging time period is between 12:00∼14:00.

2) The conventional load at each node is equal to the base load between 12:00∼13:00 and that of 80% base load between 13:00∼14:00. The power factor is 0.95.

3) The power prices in the time range of 12:00∼13:00 and 13:00∼14:00 are 0.8 and 0.4 Yuan/kWh, respectively.

4) All EVs adopt the three-phase charging mode.

5) The charging demand of each EV is 10 kWh.

6) Minimal and maximal charging power of each EV are 0 and 10 kW, respectively.

7) The charging efficiency is set to be 1.0.

8) The optimization time interval is 1 hour.

9) The upper and lower voltage limits are 1.0 and 0.9 p.u., respectively.

2) Simulation Results: All the programs are written with MATLAB. The LP is solved by using the library function linprog. The precise model is solved by the primal dual interior point method [27]. The CPU of the computer is Intel (R) Core (TM) i3-4510. The main frequency of the CPU is 3.5 GHz with 32G RAM.

Some results are shown in Table III and Table IV, where f.0 and f.1 represent the optimization results during 12:00∼13:00 and 13:00∼14:00 solved by the simplified LP, respectively. PM.0 and PM.1 represent the optimization results during 12:00∼13:00 and 13:00∼14:00 solved by the approximate LP, respectively. PD.0 and PD.1 represent the optimization results during 12:00∼13:00 and 13:00∼14:00 solved by the precise nonlinear model, respectively. Pf.0 and Pf.1 represent

TABLE I
Line Impedance of IEEE 33-Node Distribution Network

Line i∼j		Z_{aa} (Ω)	Z_{bb} (Ω)	Z_{cc} (Ω)	Z_{ab} (Ω)	Z_{ac} (Ω)	Z_{bc} (Ω)
33∼1	Real	0.0935	0.0933	0.0931	0.0009	0.0013	0.0011
	Imag	0.0477	0.0475	0.0474	0.0004	0.0007	0.0005
1∼2	Real	0.5003	0.4989	0.4979	0.0049	0.0073	0.0059
	Imag	0.2548	0.2541	0.2536	0.0025	0.0037	0.0030
2∼3	Real	0.3714	0.3704	0.3696	0.0036	0.0054	0.0043
	Imag	0.1891	0.1886	0.1882	0.0018	0.0027	0.0022
3∼4	Real	0.3868	0.3856	0.3849	0.0038	0.0057	0.0045
	Imag	0.1970	0.1964	0.1960	0.0019	0.0029	0.0023
4∼5	Real	0.8312	0.8288	0.8271	0.0081	0.0122	0.0098
	Imag	0.7176	0.7154	0.7140	0.0070	0.0106	0.0084
5∼6	Real	0.1900	0.1894	0.1890	0.0018	0.0028	0.0022
	Imag	0.6280	0.6262	0.6249	0.0061	0.0092	0.0074
6∼7	Real	0.7220	0.7199	0.7185	0.0071	0.0106	0.0085
	Imag	0.2386	0.2379	0.2374	0.0023	0.0035	0.0028
7∼8	Real	1.0454	1.0423	1.0403	0.0103	0.0154	0.0123
	Imag	0.7510	0.7488	0.7473	0.0074	0.0110	0.0088
8∼9	Real	1.0596	1.0565	1.0544	0.0104	0.0156	0.0125
	Imag	0.7510	0.7488	0.7473	0.0074	0.0110	0.0088
9∼10	Real	0.1995	0.1989	0.1985	0.0019	0.0029	0.0023
	Imag	0.0659	0.0657	0.0656	0.0006	0.0009	0.0007
10∼11	Real	0.3800	0.3788	0.3781	0.0037	0.0056	0.0044
	Imag	0.1256	0.1252	0.1250	0.0012	0.0018	0.0014
11∼12	Real	1.4900	1.4856	1.4826	0.0146	0.0220	0.0176
	Imag	1.1723	1.1688	1.1665	0.0115	0.0173	0.0138
12∼13	Real	0.5497	0.5480	0.5470	0.0054	0.0081	0.0064
	Imag	0.7235	0.7214	0.7200	0.0071	0.0106	0.0085
13∼14	Real	0.5998	0.5980	0.5969	0.0059	0.0088	0.0070
	Imag	0.5338	0.5323	0.5312	0.0052	0.0078	0.0063
14∼15	Real	0.7514	0.7491	0.7477	0.0074	0.0111	0.0088
	Imag	0.5531	0.5515	0.5544	0.0054	0.0081	0.0065
15∼16	Real	1.3083	1.3044	1.3018	0.0128	0.0193	0.0154
	Imag	1.7468	1.7416	1.7382	0.0172	0.0258	0.0206
16∼17	Real	0.7429	0.7407	0.7393	0.0073	0.0109	0.0087
	Imag	0.5826	0.5808	0.5797	0.0057	0.0086	0.0068
17∼18	Real	0.1664	0.1659	0.1656	0.0016	0.0024	0.0019
	Imag	0.1588	0.1583	0.1580	0.0015	0.0023	0.0018
18∼19	Real	1.5267	1.5222	1.5192	0.0150	0.0225	0.0180
	Imag	1.3757	1.3716	1.3689	0.0135	0.0203	0.0162
19∼20	Real	0.4156	0.4144	0.4135	0.0040	0.0061	0.0049
	Imag	0.4855	0.4841	0.4831	0.0047	0.0071	0.0057
20∼21	Real	0.7195	0.7174	0.7159	0.0070	0.0106	0.0085
	Imag	0.9513	0.9485	0.9466	0.0093	0.0140	0.0112
21∼22	Real	0.4579	0.4566	0.4557	0.0045	0.0067	0.0054
	Imag	0.3129	0.3119	0.3113	0.0030	0.0046	0.0036
22∼23	Real	0.9114	0.9087	0.9069	0.0089	0.0134	0.0107
	Imag	0.7197	0.7176	0.7161	0.0070	0.0106	0.0085
23∼24	Real	0.9094	0.9067	0.9049	0.0089	0.0134	0.0107
	Imag	0.7116	0.7095	0.7081	0.0070	0.0105	0.0084
24∼25	Real	0.2060	0.2054	0.2050	0.0020	0.0030	0.0024
	Imag	0.1049	0.1046	0.1044	0.0010	0.0015	0.1044
25∼26	Real	0.2884	0.2876	0.2870	0.0028	0.0042	0.0034
	Imag	0.1468	0.1464	0.1461	0.0014	0.0021	0.0017
26∼27	Real	1.0748	1.0717	1.0695	0.0105	0.0158	0.0127
	Imag	0.9477	0.9449	0.9430	0.0093	0.0140	0.0112
27∼28	Real	0.8162	0.8138	0.8122	0.0080	0.0120	0.0096
	Imag	0.7111	0.7090	0.7076	0.0070	0.0105	0.0084
28∼29	Real	0.5151	0.5135	0.5125	0.0050	0.0076	0.0060
	Imag	0.2623	0.2616	0.2610	0.0025	0.0038	0.0031
29∼30	Real	0.9890	0.9860	0.9841	0.0097	0.0146	0.0116
	Imag	0.9774	0.9745	0.9726	0.0096	0.0144	0.0115
30∼31	Real	0.3151	0.3142	0.3136	0.0031	0.0046	0.0037
	Imag	0.3637	0.3662	0.3655	0.0036	0.0054	0.0043
31∼32	Real	0.3461	0.3450	0.3444	0.0034	0.0051	0.0040
	Imag	0.5381	0.5365	0.5355	0.0053	0.0079	0.0063

TABLE II
LOAD OF IEEE 33-NODE DISTRIBUTION SYSTEM

Node	Phase A [kW]	Phase B [kW]	Phase C [kW]
1	32 + 19i	33 + 20i	35 + 21i
2	30 + 13i	31 + 15i	29 + 13i
3	45 + 30i	0 + 0i	35 + 24i
4	20 + 10i	20 + 10i	20 + 10i
5	20 + 6i	20 + 7i	20 + 7i
6	65 + 33i	70 + 34i	65 + 33i
7	70 + 34i	65 + 33i	65 + 33i
8	20 + 7i	18 + 6i	22 + 7i
9	21 + 7i	20 + 7i	0+ 0i
10	14 + 9i	16 + 11i	15 + 10i
11	20 + 11i	20 + 12i	20 + 12i
12	21 + 12i	19 + 11i	20 + 12i
13	40 + 28i	38 + 27i	42 + 25i
14	0 + 0i	19 + 3i	20 + 3i
15	19 + 6i	20 + 7i	21 + 7i
16	19 + 6i	21 + 7i	20 + 7i
17	30 + 14i	30 + 13i	30 + 13i
18	33 + 15i	29 + 13i	28 + 12i
19	29 + 13i	28 + 12i	33 + 15i
20	29 + 12i	30 + 13i	31 + 15i
21	28 + 12i	33 + 15i	29 + 13i
22	30 + 16i	31 + 17i	29 + 17i
23	130 + 60i	140+ 70i	150+ 70i
24	150+ 70i	130+ 70i	140+ 60i
25	20 + 8i	20 + 8i	20 + 9i
26	18 + 7i	22 + 9i	20 + 9i
27	19 + 6i	22 + 8i	19 + 6i
28	38 + 23i	42 + 25i	40 + 22i
29	60 + 180i	70 + 210i	70 + 210i
30	45 + 20i	51 + 23i	54 + 27i
31	70 + 33i	72 + 35i	68 + 32i
32	20 + 13i	20 + 14i	20 + 13i

TABLE III
OPTIMAL CHARGING POWER FOR DIFFERENT METHODS IN CASE 1

Nodes	17	21	24.	32	Computational Time [s]
f.0 [kW]	56.8	0	0	0	0.130
f.1 [kW]	343.2	400	400	400	
PM.0 [kW]	111	0	0	0	0.198
PM.1 [kW]	289	400	400	400	
PD.0 [kW]	111.4	0	0	0	8.295
PD.1 [kW]	288.6	400	400	400	

voltages of power flow calculations during 12:00∼13:00 and 13:00∼14:00, by substituting the optimal charging power of EVs using the simplified LP into the precise power flow equations, respectively. PF.0 and PF.1 represent voltages of power flow calculations during 12:00∼13:00 and 13:00∼14:00, by substituting the optimal charging power of EVs using the approximate LP into the precise power flow equations, respectively.

As can be seen in Table III and Table IV, the results obtained by the simplified and approximate LP are relatively close. Thus, the result is of high precision via the initial point obtained by the simplified LP for linearizing the nonlinear terms of branch flow equations. Moreover, the optimization results obtained by the approximate LP are very close to those of the primal dual interior point method. This observation demonstrates that the proposed method has a high precision. However, the computational speed of the proposed method is about 40 times higher than that of the primal dual interior point method. As can be seen from the results of power flow

TABLE IV
OPTIMAL VOLTAGES FOR DIFFERENT METHODS IN CASE 1

Nodes	17	21	24	32
f.0 [p.u.]	0.9168	0.9921	0.9704	0.9229
	0.9120	0.9917	0.9707	0.9172
	0.9137	0.9916	0.9702	0.9195
f.1 [p.u.]	0.9041	0.9858	0.9663	0.9148
	0.9000	0.9854	0.9665	0.9099
	0.9016	0.9854	0.9661	0.9124
PM.0 [p.u.]	0.9099	0.9919	0.9693	0.9194
	0.9044	0.9914	0.9695	0.9131
	0.9064	0.9914	0.9690	0.9158
PM.1 [p.u.]	0.9045	0.9855	0.9653	0.9122
	0.9000	0.9851	0.9655	0.9069
	0.9017	0.9851	0.9651	0.9096
PD.0 [p.u.]	0.9098	0.9919	0.9693	0.9194
	0.9043	0.9914	0.9695	0.9131
	0.9063	0.9914	0.9690	0.9157
PD.1 [p.u.]	0.9045	0.9856	0.9654	0.9122
	0.9000	0.9851	0.9655	0.9069
	0.9017	0.9851	0.9651	0.9096
Pf.0 [p.u.]	0.9142	0.9919	0.9695	0.9203
	0.9087	0.9915	0.9697	0.9140
	0.9107	0.9914	0.9692	0.9167
Pf.1 [p.u.]	0.9000	0.9855	0.9651	0.9113
	0.8954	0.9851	0.9653	0.9059
	0.8971	0.9851	0.9649	0.9086
PF.0 [p.u.]	0.9098	0.9919	0.9693	0.9194
	0.9043	0.9914	0.9695	0.9131
	0.9063	0.9914	0.9690	0.9157
PF.1 [p.u.]	0.9045	0.9856	0.9654	0.9122
	0.9000	0.9851	0.9655	0.9068
	0.9017	0.9851	0.9651	0.9096

calculation in Table IV, the optimal charging power obtained by the simplified LP may result in voltages dropping out of the lower limit (see the bold font). However, for the approximate LP, voltage results of the power flow calculation are very close to those of the optimization results. Furthermore, all of the voltages are within the rated range.

B. Case 2

1) Simulation Conditions: In this case, all the EVs are assumed to adopt the single-phase charging mode to testify the capabilities of the proposed method. The simulation platform is the same as that of case 2 in [28]. Time-of-use electricity prices are set as 0.8, 0.4 Yuan/kWh during 12:00∼13:00 and 13:00∼14:00, respectively. The conventional household loads at each node of each phase are 4.5 and 3.6 kW during 12:00∼13:00 and 13:00∼14:00, respectively. The charging demand of each EV is 5 kWh. The maximum charging power is 4 kW. Other simulation conditions are set as same as those of case 2 in [28].

2) Simulation Results: All the programs are written with MATLAB. The simplified and approximate LP is solved using library function linprog. The precise model is solved by the primal dual interior point method [27]. The computer configuration is the same as that in case 1. Simulation results of different optimization algorithms are shown in Table V and Table VI. It can be seen that results of the proposed method are in good agreement with those of the primal dual interior point method. However, the computational speed is significantly superior to the primal dual interior point method.

TABLE V
OPTIMAL CHARGING POWER FOR DIFFERENT METHODS IN CASE 2

Nodes	6	7	11	12	Computational Time [s]
f.0 [p.u.]	0.0188	0.0188	0.0188	0.0188	0.103
f.1 [p.u.]	0.0750	0.0750	0.0750	0.0750	
PM.0 [p.u.]	0.0188	0.0188	0.0188	0.0188	0.161
PM.1 [p.u.]	0.0750	0.0750	0.0750	0.0750	
PD.0 [p.u.]	0.0188	0.0188	0.0188	0.0188	1.390
PD.1 [p.u.]	0.0750	0.0750	0.0750	0.0750	

TABLE VI
OPTIMAL VOLTAGE FOR DIFFERENT METHODS IN CASE 2

Nodes	6	7	11	12
f.0 [p.u.]	0.9285	0.9358	0.9338	0.9348
	0.9378	0.9428	0.9429	0.9404
	0.9334	0.9429	0.9396	0.9418
f.1 [p.u.]	0.9187	0.9260	0.9231	0.9263
	0.9554	0.9539	0.9595	0.9489
	0.9382	0.9543	0.9464	0.9545
PM.0 [p.u.]	0.9216	0.9290	0.9270	0.9280
	0.9322	0.9373	0.9375	0.9349
	0.9275	0.9371	0.9338	0.9360
PM.1 [p.u.]	0.9093	0.9167	0.9138	0.9171
	0.9516	0.9501	0.9557	0.9448
	0.9329	0.9493	0.9414	0.9495
PD.0 [p.u.]	0.9209	0.9284	0.9263	0.9273
	0.9317	0.9368	0.9370	0.9344
	0.9271	0.9367	0.9334	0.9357
PD.1 [p.u.]	0.9082	0.9157	0.9128	0.9160
	0.9512	0.9497	0.9553	0.9444
	0.9331	0.9494	0.9415	0.9496
PF.0 [p.u.]	0.9215	0.9289	0.9269	0.9278
	0.9318	0.9370	0.9370	0.9346
	0.9274	0.9369	0.9337	0.9358
PF.1 [p.u.]	0.9082	0.9157	0.9128	0.9160
	0.9512	0.9497	0.9553	0.9444
	0.9331	0.9494	0.9415	0.9496

C. Case 3

1) Simulation Conditions: In this case, the coexistence of the single- and three-phase charging modes for EVs in the distribution system to test the capabilities of the proposed method. Simulation conditions are the same as those in case 2 except that EVs connected to nodes 3, 4, 5, 8, 9, and 10 adopt the three-phase charging mode and the maximum charging power of each EV is 12 kW.

2) Simulation Results: The optimal charging power of EVs at different nodes with different algorithms and the computational time of the program are shown in Table VII. As can be seen, the computational efficiency of the proposed method is slightly better than that of case 2. This is because we choose the total power rather than the single-phase charging power for EV with the three-phase charging mode as the optimization variable. The charging power of each phase is one-third of this variable. That is, with some simple mathematical techniques, the number of optimization variables, equality and inequality constraints can be the same as those in case 2. The imbalance of the distribution system is reduced compared with that of case 2 due to the existence of three-phase charging mode. Thus, the numerical stability of the program is improved and the computational speed is slightly higher than that of case 2. The voltage results using different optimization algorithms are similar with those in Table VI. Based on simulation results, we can draw the same conclusions as case 2.

TABLE VII
OPTIMAL CHARGING POWER FOR DIFFERENT METHODS WITH SINGLE- AND THREE-PHASE CHARGING COEXISTING

Nodes	5	6	10	11	Computational Time [s]
f.0 [p.u.]	0.0000	0.0188	0.0000	0.0188	0.093
f.1 [p.u.]	0.0939	0.0750	0.0939	0.0750	
PM.0 [p.u.]	0.0000	0.0188	0.0000	0.0188	0.150
PM.1 [p.u.]	0.0939	0.0750	0.0936	0.0750	
PD.0 [p.u.]	0.0000	0.0188	0.0000	0.0188	1.397
PD.1 [p.u.]	0.0936	0.0750	0.0936	0.0750	

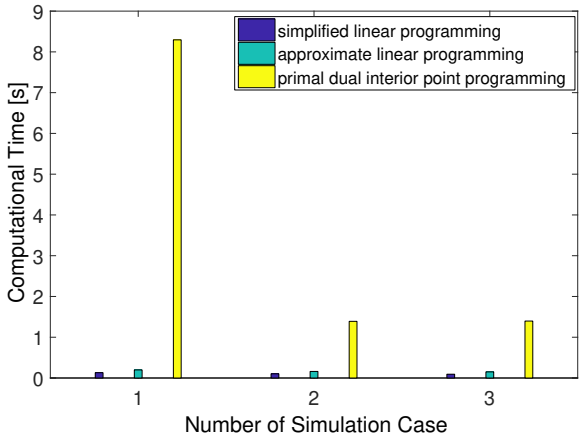

Fig. 4. Computational efficiency with different methods.

The computational time of aforementioned three cases with different optimization methods are shown in Fig. 4. As can be seen, the calculation efficiency of the proposed method is significantly better than that of the primal dual interior point method and slightly worse than that of the simplified LP. However, the precision is very close to the primal dual interior point method.

D. Case 4

1) Simulation Conditions: A 354-node distribution system is used to test the capabilities of the proposed method. As shown in Fig. 5, the MV distribution system is a 34-node distribution system and the rated phase to ground voltage is 13.8 kV. There are 16 low voltage (LV) distribution systems in the simulation platform. The topology of each one is shown in Fig. 6. The rated phase-to-ground voltage is 220 V. In Fig. 6, the capacity of the transformer is 250 kVA and the terminal node 'xx' is connected to the MV distribution system at nodes 11, 13, 14, 17, 18, 20, 22, 24-26, and 28-33, respectively. The rated currents of the cables in the MV and LV distribution networks are 200 A and 368 A, respectively. There is a conventional household load connected to each node in the LV distribution system and each household has one EV connected. Node 34 is taken as the slack node and its voltage is kept to be 1.1 p.u.. The rest of nodes are taken as PQ nodes. The single-phase base power and voltages are chosen to be 1000 kVA, 13.8 kV and 0.22 kV, respectively. The back forward sweep method is used to calculate the power flow.

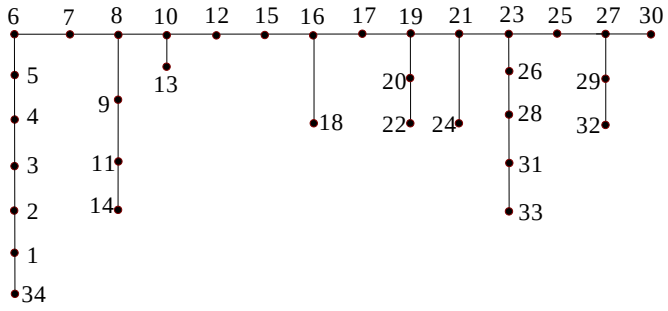

Fig. 5. MV distribution system.

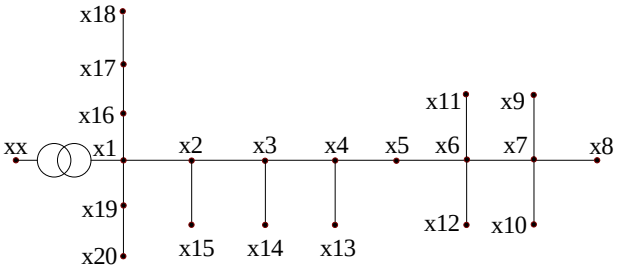

Fig. 6. LV distribution system.

Other simulation conditions are set as follows:

1) All EV owners are willing to participate in the coordinated charging and charging power of each EV is fully controllable. The charging time period is between 18:00∼8:00.

2) The conventional house hold load at each node is set to be the same.

3) At 18:00∼19:00, the conventional household load connected to phases A, B, C are 0.8666, 0.8000, and 0.7334 kW, respectively. Power factor is set to be 0.95. The conventional household load model is set to be 60% constant power load plus 40% constant impedance load.

4) All EV adopt three-phase charging mode.

5) Charging demand of each EV is 15 kWh.

6) Minimal and maximal charging power of each EV is 0 and 10 kW, respectively.

7) Charging efficiency is set to be 1.0.

8) The optimization time interval is 1 hour.

9)The upper and lower voltage limits are 1.1 and 0.9 p.u., respectively.

2) Simulation Results: We utilize MATLAB to call the cplex LP library function cplexlp for the optimization calculation. The configuration of computer is the same as that in case 1. During the optimization period, the total conventional load and charging load obtained by the simplified and approximate LP are denoted as blue, orange, and yellow boxes, respectively, as shown in Fig. 7. As can be seen, all of EVs are only charged during 4:00∼6:00, when the electricity prices are relatively low. However, the total charging power difference between the simplified and approximate LP is significant. Moreover, since the lowest electricity price and conventional load level occur during 5:00∼6:00, the total charging load is the maximal during 5:00∼6:00. The electricity price during 4:00∼5:00 is higher than that during 6:00∼7:00. The total charging load

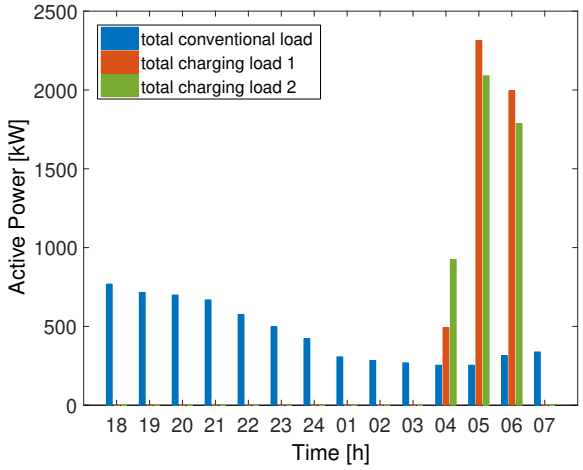

Fig. 7. Total load at different time periods.

during 4:00∼5:00 is much lower than that during 6:00∼7:00. This is because most of the charging loads are supplied during 5:00∼7:00 by the optimization programming.

Let the cable connected with the root node of the distribution system and that connected with the LV side of the transformer be called the MV and LV main cables, respectively. The loading of the MV and LV main cables and transformer for phase A are shown in Fig. 8. Clearly, the loadings of transformer and cables are low when the electricity price is high. Because EVs are not charged when the electricity price is high. Otherwise, the loadings of transformer and cables are high when the electricity price is low. Because EVs are charged with high power when the electricity price is low. During 5:00∼6:00, since the electricity price is minimal, the total charging power of EV is maximal. As a result, the loadings of transformer and main cable are the largest during 5:00∼6:00. However, under both circumstances, the loadings of transformer and cables are not more than 90%. The capacity of the distribution system equipments is more than sufficient to accommodate the charging load. Moreover, the branch flows obtained by the simplified and approximate LP are very close. Thus, it is reasonable to take the results obtained by the simplified LP as the initial point for linearizing the nonlinear terms of the branch flow equations.

Both minimum voltages of each time period obtained by the simplified and approximate LP are shown in Fig. 9a. Compared with Fig. 7, both the minimum voltages are high when the total load is low. Otherwise, the minimum voltages are low when the total load is high. The minimum voltage is always within the rated range during the optimization time periods. The minimum voltages of power flow calculation results using the optimal charging power obtained by the simplified and approximate LP are shown in Fig. 9b. Since the voltage and power losses are ignored in the simplified LP, the minimum voltage of the power flow calculation drops to 0.8651 p.u. and 0.8659 p.u. during 5:00∼6:00 and 6:00∼7:00, respectively. Thus, the optimal charging power obtained by the simplified LP is not able to meet the node voltage constraint. That is, the optimal charging power obtained by simplified

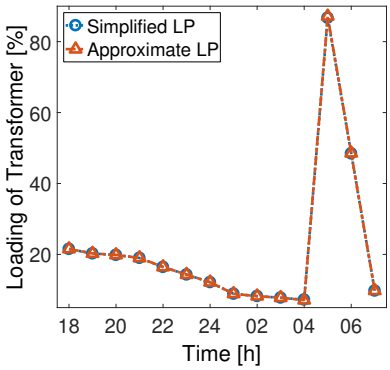

(a) Active power loading of transformer at node 11

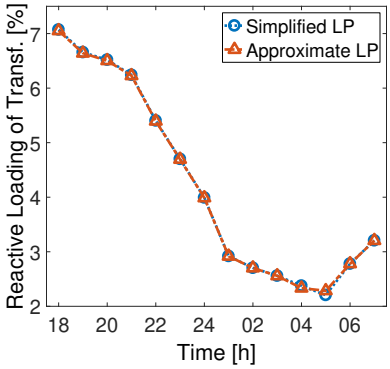

(b) Reactive power loading of transformer at node 11

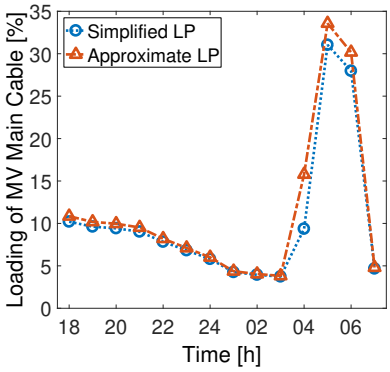

(c) Loading of main cable at node 33

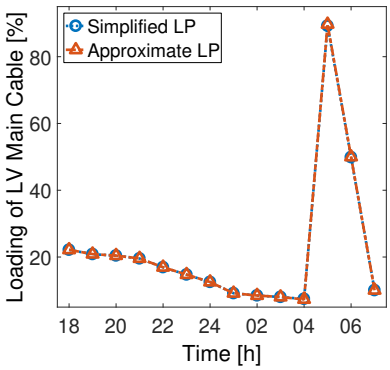

(d) Active power loading of main cable at node 11

Fig. 8. Loadings of electric equipments on phase A.

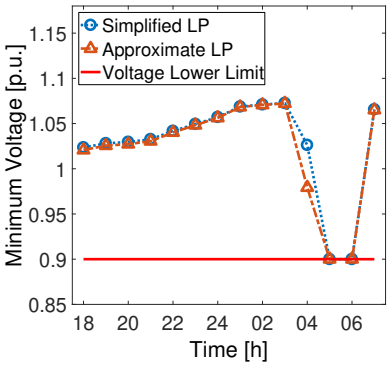

(a) Solving the model

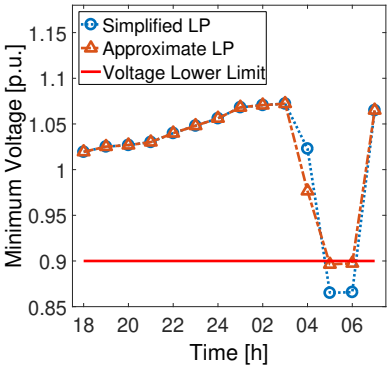

(b) Power flow calculation

Fig. 9. Minimum voltage comparison at each time period.

LP may be unfeasible. As the voltage constraint has been loosened, too many EVs are charged with high power during the lowest electricity price time periods during 5:00∼6:00 and 6:00∼7:00 by simplified LP. However, based on the optimal charging power obtained by the approximate LP, the minimum voltages during 5:00∼6:00 and 6:00∼7:00 are 0.8963 p.u. and 0.8975 p.u., respectively. This result can approximately meet the node voltage constraint. Overall, this observation can demonstrate that the proposed linearization strategy has a high precision.

The optimal charging power of EVs that are nearest and farthest from the root node is shown in Fig. 10. When the electricity price is low during 4:00∼7:00, the charging power is close to its maximum value. When the electricity price is high during 18:00∼3:00 and 7:00∼8:00, the charging power is zero. Since EVs nearest from the root node are charged with the maximum power at the lowest price during 5:00∼7:00, those farthest from the root node can be charged at the maximum power during 4:00∼5:00 when the conventional load level is the lowest rather than 5:00∼7:00. Thus, voltages cannot drop out of the lower limit. The charging power of EV is determined firstly by electricity price and then by charging location. Although the electricity is the lowest during 5:00∼6:00, the charging power of the EV farthest from the root node is zero. This is because too many EVs in front of it have been charged with high power. In a conclusion, in order not to exceed the voltage magnitude limit, charging power of EVs at the end of distribution systems sometimes must be charged with low power during low electricity price.

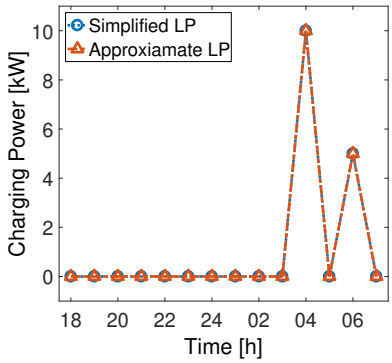

(a) EV farthest from the root node

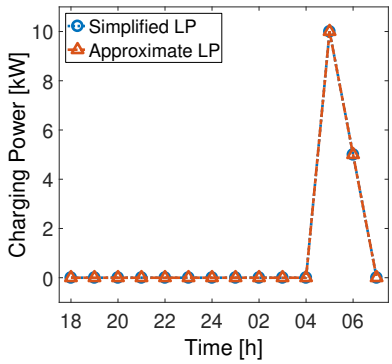

(b) EV nearest from the root node

Fig. 10. Optimal charging power of EVs in the distribution system.

3) Comparison with Selected Method: As can be seen in Fig. 7–Fig. 10, all the EVs are only charged during 4:00∼7:00 and the charging power is zero during other time periods. Thus, for the third and forth steps in Fig. 2, the linearization and optimization time periods can be reduced to 4:00∼7:00. Hence, the computational speed can be further improved. The optimization results of the proposed method are compared with those in [16] and shown in Table VIII. As can be seen, the computational speed of the proposed method is much faster than that of [16]. This is because the model formulated in this paper is based on the branch flow equation. The optimization variables do not contain the branch current and the phase angle of the node voltage. However, the model in [16] adopts the current type power flow equation in the Cartesian coordinate system. Many variables and constraints are introduced to linearize the branch current constraint. The number of variables in [16] is several times of the proposed model. The number of branch current and node voltage constraints in [16] is more than 10 times and 5 times of the proposed method. This results in a significant increase of the computational time. In addition, discrete variables are also introduced in [16] and makes the model non-convex. Also, this can significantly increase the total computational time.

VII. Conclusions and Discussion

In this paper, branch flow equations of balanced and unbalanced distribution systems are derived. The model for coordinated charging of EVs is proposed to minimize the total charging cost of holders. The charging demand, three-phase imbalance of distribution network, voltage and power flow constraints are considered. The linearization method is proposed for nonlinear terms of branch flow equations to develop a fast solving strategy. Via linearizing nonlinear terms of branch flow equations, the first stage linear programming (LP) is formulated to calculate the estimated branch power and node voltages as initial points. The second stage LP is formulated to calculate the optimal charging power based on linearized branch flow equations. Both the high computational speed and precision of the proposed method are verified by two case studies. The fast calculation speed and high precision of the proposed method are verified by four test cases as shown in Tables III–VIII, Fig. 4, and Fig. 9.

TABLE VIII
Comparison With the Model in [16]

Metrics	Method in [16]	Proposed Method	
		Second Stage Within 14 hours	Second Stage Within 3 hours
Objective Function [Yuan]	850.64	848.92	848.92
Minimum Voltage [p.u.]	0.90	0.90	0.90
Computational Time [s]	1360	212	114

In this paper, the simulation time interval is set to 1 hour. Considering the practical application, it should be highlighted that it can be reduced to 15 minutes or even 3 to 5 minutes. Therefore, forecasting precision can be improved and uncertainties of EVs and conventional load can be considered by using online rolling optimization and fast charging EVs can be taken into account so as to avoid voltage beyond lower limit and branch overloading caused by fast charging of EVs. Under this circumstance, the capability of fast computational speed of the proposed method can be further reflected. This is because the computational speed of the proposed method is just slightly slower than that of the conventional LP. The proposed method is also applicable to other objective functions such as minimization of network losses or total electricity costs of distribution system operator.

The main contribution of this paper is that we have proposed a fast solution method for EVCC problem. All simulation systems are based on actual or IEEE standard distribution networks. The setting of other simulation conditions is also reasonable, which can fully demonstrate the effectiveness of the proposed method. The simulation conditions in case 4 are almost the same as those in reference [16], but the calculation speed is much faster than that in reference [16]. Four simulation cases in this paper show that the proposed method has excellent capabilities - high accuracy and fast speed. Even if the access and departure time and charging demand of EVs are changed, the proposed method is still applicable. In future work, more realistic EV user behavior and laboratory scale testing will be carried out to validate the capabilities of the proposed method.

In future work, the proposed method can also be applicable to other objective functions, such as the minimization of network losses and total electricity cost for distribution system

operators.

ACKNOWLEDGMENT

This work was supported by the National Natural Science Foundations of China (under Grant No. 51577046 and 51107090), the National Defense Advanced Research Project (under Grant No. C1120110004 and 9140A27020211DZ5102), the Key Grant Project of Chinese Ministry of Education (under Grant No. 313018), the Anhui Provincial Science and Technology Foundation of China (under Grant No. 1301022036), the National Research Foundation for the Doctoral Program of Higher Education of China (under Grant No. JZ2015HGBZ0095), the State Key Program of National Natural Science of China (under Grant No. 51637004), and the National Key Research and Development Plan "Important Scientific Instruments and Equipment Development" (under Grant 2016YFF0102200). The authors would also like to thank the anonymous reviewers for their constructive suggestions to this research.

REFERENCES

[1] L. Cheng, Y. Chang, and R. Huang, "Mitigating voltage problem in distribution system with distributed solar generation using electric vehicles," *IEEE Trans. Sustain. Energy*, vol. 6, no. 4, pp. 1475–1484, 2015.

[2] Y. P. Agalgaonkar, B. C. Pal, and R. A. Jabr, "Distribution voltage control considering the impact of PV generation on tap changers and autonomous regulators," *IEEE Trans. Power Syst.*, vol. 29, no. 1, pp. 182–192, 2014.

[3] J. Zhang, M. Cui, H. Fang, and Y. He, "Two novel load balancing platforms using common DC buses," *IEEE Trans. Sustain. Energy*, 2017, in press.

[4] J. Zhang, X. Yuan, and Y. Yuan, "A novel genetic algorithm based on all spanning trees of undirected graph for distribution network reconfiguration," *J. Mod. Power Syst. Clean Energy*, vol. 2, no. 2, pp. 143–149, 2014.

[5] W. Zheng, W. Wu, B. Zhang, Z. Li, and Y. Liu, "Fully distributed multi-area economic dispatch method for active distribution networks," *IET Gener. Transm. Distrib.*, vol. 9, no. 12, pp. 1341–1351, 2015.

[6] W. Zheng, W. Wu, B. Zhang, H. Sun, and Y. Liu, "A fully distributed reactive power optimization and control method for active distribution networks," *IEEE Trans. Smart Grid*, vol. 7, no. 2, pp. 1021–1033, 2016.

[7] S. D. Manshadi, M. E. Khodayar, K. Abdelghany, and H. Üster, "Wireless charging of electric vehicles in electricity and transportation networks," *IEEE Trans. Smart Grid*, vol. 9, no. 5, pp. 4503–4512, 2018.

[8] M. Singh, P. Kumar, and I. Kar, "Implementation of vehicle to grid infrastructure using fuzzy logic controller," *IEEE Trans. Smart Grid*, vol. 3, no. 1, pp. 565–577, 2012.

[9] O. Beaude, Y. He, and M. Hennebel, "Introducing decentralized EV charging coordination for the voltage regulation," in *Innovative Smart Grid Technologies Europe (ISGT EUROPE), 2013 4th IEEE/PES*. IEEE, 2013, pp. 1–5.

[10] L. Gan, U. Topcu, and S. H. Low, "Optimal decentralized protocol for electric vehicle charging," *IEEE Trans. Power Syst.*, vol. 28, no. 2, pp. 940–951, 2013.

[11] S. Deilami, A. S. Masoum, P. S. Moses, and M. A. Masoum, "Real-time coordination of plug-in electric vehicle charging in smart grids to minimize power losses and improve voltage profile," *IEEE Trans. Smart Grid*, vol. 2, no. 3, pp. 456–467, 2011.

[12] A. S. Masoum, S. Deilami, P. Moses, M. Masoum, and A. Abu-Siada, "Smart load management of plug-in electric vehicles in distribution and residential networks with charging stations for peak shaving and loss minimisation considering voltage regulation," *IET Gener. Transm. Distrib.*, vol. 5, no. 8, pp. 877–888, 2011.

[13] K. Clement-Nyns, E. Haesen, and J. Driesen, "The impact of charging plug-in hybrid electric vehicles on a residential distribution grid," *IEEE Trans. Power Syst.*, vol. 25, no. 1, pp. 371–380, 2010.

[14] P. Richardson, D. Flynn, and A. Keane, "Optimal charging of electric vehicles in low-voltage distribution systems," *IEEE Trans. Power Syst.*, vol. 27, no. 1, pp. 268–279, 2012.

[15] P. Richardson, D. Flynn, and A. Keane, "Local versus centralized charging strategies for electric vehicles in low voltage distribution systems," *IEEE Trans. Smart Grid*, vol. 3, no. 2, pp. 1020–1028, 2012.

[16] J. F. Franco, M. J. Rider, and R. Romero, "A mixed-integer linear programming model for the electric vehicle charging coordination problem in unbalanced electrical distribution systems," *IEEE Trans. Smart Grid*, vol. 6, no. 5, pp. 2200–2210, 2015.

[17] Y. He, B. Venkatesh, and L. Guan, "Optimal scheduling for charging and discharging of electric vehicles," *IEEE Trans. Smart Grid*, vol. 3, no. 3, pp. 1095–1105, 2012.

[18] J. Hu, S. You, M. Lind, and J. Ostergaard, "Coordinated charging of electric vehicles for congestion prevention in the distribution grid," *IEEE Trans. Smart Grid*, vol. 5, no. 2, pp. 703–711, 2014.

[19] S. Weckx and J. Driesen, "Load balancing with EV chargers and PV inverters in unbalanced distribution grids," *IEEE Trans. Sustain. Energy*, vol. 6, no. 2, pp. 635–643, 2015.

[20] E. Sortomme, M. M. Hindi, S. J. MacPherson, and S. Venkata, "Co-ordinated charging of plug-in hybrid electric vehicles to minimize distribution system losses," *IEEE Trans. Smart Grid*, vol. 2, no. 1, pp. 198–205, 2011.

[21] P. Staats, W. Grady, A. Arapostathis, and R. Thallam, "A procedure for derating a substation transformer in the presence of widespread electric vehicle battery charging," *IEEE Transactions on Power Delivery*, vol. 12, no. 4, pp. 1562–1568, 1997.

[22] R.-C. Leou, C.-L. Su, and C.-N. Lu, "Stochastic analyses of electric vehicle charging impacts on distribution network," *IEEE Transactions on Power Systems*, vol. 29, no. 3, pp. 1055–1063, 2014.

[23] J. D. Melo, E. M. Carreno, and A. Padilha-Feltrin, "Spatial-temporal simulation to estimate the load demand of battery electric vehicles charging in small residential areas," *Journal of Control, Automation and Electrical Systems*, vol. 25, no. 4, pp. 470–480, 2014.

[24] K. Qian, C. Zhou, M. Allan, and Y. Yuan, "Modeling of load demand due to EV battery charging in distribution systems," *IEEE Transactions on Power Systems*, vol. 26, no. 2, pp. 802–810, 2011.

[25] A. Lojowska, D. Kurowicka, G. Papaefthymiou, L. van der Sluis *et al.*, "Stochastic modeling of power demand due to EVs using copula," *IEEE Transactions on Power Systems*, vol. 27, no. 4, p. 1960, 2012.

[26] B. A. Robbins and A. D. Domínguez-García, "Optimal reactive power dispatch for voltage regulation in unbalanced distribution systems," *IEEE Trans. Power Syst.*, vol. 31, no. 4, pp. 2903–2913, 2016.

[27] J. Zhang, Y. He, M. Cui, and Y. Lu, "Primal dual interior point dynamic programming for coordinated charging of electric vehicles," *J. Mod. Power Syst. Clean Energy*, vol. 5, no. 6, pp. 1004–1015, 2017.

[28] J. Zhang, M. Cui, H. Fang, and Y. He, "Smart charging of EVs in residential distribution systems using the extended iterative method," *Energies*, vol. 9, no. 12, pp. 985–999, 2016.

Jian Zhang received the B.S., M.S., and Ph.D. degrees from Wuhan University, Wuhan, China, all in Electrical Engineering and Automation, in 2005, 2007, and 2011, respectively.

Currently, he works as a Lecturer at Hefei University of Technology. His research interests include load modeling, renewable distributed generation, and distributed network technology.

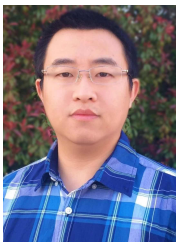

Mingjian Cui (S'12–M'16–SM'18) received the B.S. and Ph.D. degrees from Wuhan University, Wuhan, Hubei, China, all in Electrical Engineering and Automation, in 2010 and 2015, respectively.

Currently, he is a Research Assistant Professor at Southern Methodist University, Dallas, Texas, USA. He was also a Visiting Scholar from 2014 to 2015 in the Transmission and Grid Integration Group at the National Renewable Energy Laboratory (NREL), Golden, Colorado, USA. His research interests include power system operation, wind and solar forecasts, machine learning, data analytics, and statistics. He has authored/coauthored over 50 peer-reviewed publications. Dr. Cui serves as an Associate Editor for the journal of IET Smart Grid and Journal of Computer Science Research. He is also the Best Reviewer of the IEEE Transactions on Smart Grid for 2018.

Bing Li received the B.E. degree in automobile engineering from Chongqing Science and Technology University, Chongqing, China, in 1995, and the M.E. and Ph.D. degrees in electrical engineering from Hunan University, Changsha, China, in 2006 and 2011, respectively.

He has been a Post-Doctoral Researcher and a Visiting Scholar with the College of Electrical and Information Engineering, Hunan University, since 2011. He has been an Associate Professor with the School of Electrical and Automation Engineering, Hefei University, Hefei, China, since 2013. His current research interests include radio frequency identification technology, wireless sensor networks, and signal processing.

Hualiang Fang received the B.S., M.S., and Ph.D. degrees all in Electrical and Electronic Engineering from Huazhong University of Science and Technology, Wuhan, China, in 1999, 2003, and 2006, respectively.

Currently, he is an Associate Professor of the School of Electrical Engineering at Wuhan University. His research interests include self-healing smart grid and power system reliability.

Yigang He received the M.S. degree in electrical engineering from Hunan University, Changsha, China, in 1992 and the Ph.D. degree in electrical engineering from Xi'an Jiaotong University, Xi'an, China, in 1996. He was a Senior Visiting scholar with the University of Hertfordshire, Hatfield, U.K., in 2002. In 2011, he joined the Hefei University of Technology, China, and currently works as the Head of School of Electrical Engineering and Automation, Hefei University of Technology. He has published 200 journal and conference papers in the areas, including circuit theory and its applications, testing and fault diagnosis of analog and mixed-signal circuits, electrical signal detection, smart grid, radio frequency identification technology, and intelligent signal processing.